Journal of Hydrology 373 (2009) 545–561

Contents lists available at ScienceDirect

Journal of Hydrology

journal homepage: www.elsevier.com/locate/jhydrol

Effects of meteorological models on the solution of the surface energy balance and soil temperature variations in bare soils

Hirotaka Saito [a,*], Jiri Šimůnek [b]

[a] Department of Ecoregion Science, Tokyo University of Agriculture and Technology, 3-5-8 Saiwaicho, Fuchu, Tokyo 183-8509, Japan
[b] Department of Environmental Sciences, University of California, Riverside, California 92521, USA

ARTICLE INFO

Article history:
Received 3 July 2008
Received in revised form 14 March 2009
Accepted 23 May 2009

This manuscript was handled by P. Baveye, Editor-in-Chief, with the assistance of Stephanie Roulier, Associate Editor

Keywords:
HYDRUS–1D
Water and vapor transport
Thermal conductivity
Net radiation
Evaporation

SUMMARY

A complete evaluation of the soil thermal regime can be obtained by evaluating the movement of liquid water, water vapor, and thermal energy in the subsurface. Such an evaluation requires the simultaneous solution of the system of equations for the surface water and energy balance, and subsurface heat transport and water flow. When only daily climatic data is available, one needs not only to estimate diurnal cycles of climatic data, but to calculate the continuous values of various components in the energy balance equation, using different parameterization methods. The objective of this study is to quantify the impact of the choice of different estimation and parameterization methods, referred together to as meteorological models in this paper, on soil temperature predictions in bare soils. A variety of widely accepted meteorological models were tested on the dataset collected at a proposed low-level radioactive-waste disposal site in the Chihuahua Desert in West Texas. As the soil surface was kept bare during the study, no vegetation effects were evaluated. A coupled liquid water, water vapor, and heat transport model, implemented in the HYDRUS-1D program, was used to simulate diurnal and seasonal soil temperature changes in the engineered cover installed at the site. The modified version of HYDRUS provides a flexible means for using various types of information and different models to evaluate surface mass and energy balance. Different meteorological models were compared in terms of their prediction errors for soil temperatures at seven observation depths. The results obtained indicate that although many available meteorological models can be used to solve the energy balance equation at the soil–atmosphere interface in coupled water, vapor, and heat transport models, their impact on overall simulation results varies. For example, using daily average climatic data led to greater prediction errors, while relatively simple meteorological models may significantly improve soil temperature predictions. On the other hand, while models for the albedo and soil emissivity had little impact on soil temperature predictions, the choice of the atmospheric emissivity models had a greater impact. A comparison of all the different models indicates that the error introduced at the soil atmosphere interface propagates to deeper layers. Therefore, attention needs to be paid not only to the precise determination of the soil hydraulic and thermal properties, but also to the selection of proper meteorological models for the components involved in the surface energy balance calculations.

Introduction

A complete evaluation of the movement of liquid water, water vapor, and heat in the subsurface can be obtained by simultaneously solving the system of equations describing the surface water and energy balance, and subsurface heat transport and water flow. The use of a coupled liquid water, water vapor, and heat transport model to simulate continuous changes in water contents, soil temperatures, and a variety of fluxes has been presented by, among many others, Nassar and Horton (1989), Noborio et al. (1996a), Fayer (2000), and Saito et al. (2006). When simulations are conducted at the field scale, boundary conditions at the soil–atmosphere interface for water, vapor, and heat transport are usually determined using the surface water and energy balance (e.g., van Bavel and Hillel, 1976; Boulet et al., 1997). However, direct, continuous measurements of all the components needed to fully evaluate such surface mass and energy balances rarely exist. Usually, only standard daily climatic data from nearby weather stations and/or daily irrigation schedule are available. If detailed predictions of water and heat fluxes are needed, components of the surface mass and energy balance at much smaller time steps than those taken at daily intervals will need to be evaluated using daily standard climatic data.

The energy balance at the soil–atmosphere interface is expressed as

* Corresponding author. Tel./fax: +81 42 367 5584.
E-mail address: hiros@cc.tuat.ac.jp (H. Saito).

0022-1694/$ - see front matter © 2009 Elsevier B.V. All rights reserved.
doi:10.1016/j.jhydrol.2009.05.019

$$R_n - H - LE - G = 0 \quad (1)$$

where R_n is the net radiation (W m^{-2}), H is the sensible heat flux density (W m^{-2}), LE is the latent heat flux density (W m^{-2}), L is the latent heat (J kg^{-1}), E is the evaporation (kg m^{-2} s^{-1}), and G is the surface heat flux density (W m^{-2}). While R_n and G are positive downward, H and LE are positive upward. To solve Eq. (1) for the surface heat flux G, which is needed as the upper boundary condition in the solution of the heat transport equation, continuous variations in R_n, H, and LE must be calculated or measured. When only daily information is available, continuous values for various components in the energy balance equation must be obtained using existing estimation and parameterization methods.

Continuous diurnal cycles in climatic variables, such as air temperature, are usually generated from their mean daily values using the analogy between their cycles during the day and trigonometric functions (e.g., Jury and Horton, 2003). Once the values for air temperature, relative humidity, precipitation, and wind speed at any given time are obtained, they can be further used in parameterization formulas to calculate the components of the energy and water balance equations (Saito et al., 2006). It was not our intention to separately consider above functions and formulas. Therefore, in the remainder of this manuscript, the functions for generation of continuous diurnal cycles of climatic variables and the parameterization formulas for components of the energy balance equation are both referred to as "meteorological models". A number of comparative studies, in which measured components were compared to calculated ones, have appeared in the literature. For example, Ortega-Farias et al. (2000) compared measured and predicted air emissivities. As there are a number of available and accepted meteorological models to calculate the atmospheric variables, it is hard to determine which model is most suitable for a particular application. In addition, an extensive amount of work has been carried out over the last few decades to develop meteorological models that accurately predict evaporation rates from the soil and vegetation (e.g., Brutsaert, 1982; Monteith and Unsworth, 1990). Because of the high complexity of both air and subsurface conditions, it is extremely difficult to choose the best model to estimate evaporation rates from a particular soil. To our knowledge, the impact of the choice of particular meteorological models on simulated water flow and heat transport in the vadose zone has, so far, not been discussed or investigated. Since all the components of the surface mass and energy balance affect each other more or less in the coupled water flow and heat transport model, investigating their mutual interactions is not a straightforward task. A change in one variable can easily alter all the others.

Thus, the main objective of this study is to quantify the impact of the choice of particular meteorological models on the prediction of bare soil temperatures. We use various meteorological models in the surface energy balance equation, and then evaluate how these methods affect soil temperatures calculated with the coupled liquid water, water vapor, and heat transport model. We compare predicted soil temperatures at different soil depths with measured values. The results will allow investigators and/or practitioners to evaluate their choice of meteorological models, and provide a quantified assessment of the effects these models have on predictions of soil temperatures.

A variety of meteorological models are reviewed and tested in this study, using a dataset collected at a proposed low-level radioactive-waste disposal site in the Chihuahua Desert in West Texas, 10 km east of Sierra Blanca, where prototype engineered covers were installed (Scanlon et al., 2005). The energy balance assessment in the engineered covers is as important for evaluation of their performance as the mass (water) balance analysis. While the long-term water balance of the site was evaluated by Scanlon et al. (2005), who showed that a capillary barrier can significantly reduce drainage in arid and semi-arid regions, the energy balance of the site has not yet been fully assessed. The coupled liquid water, water vapor, and heat transport model, based on the modified HYDRUS-1D software package (Saito et al., 2006), is used in this study to simulate soil temperatures in the engineering cover, the surface of which was kept bare during the analyzed time period. The modified version of HYDRUS provides a flexible way to use various types of climatic information to evaluate surface mass and energy balance when continuous changes in water contents, temperatures, and fluxes are simulated.

Method description

Generating diurnal cycle of climatic data

The solution of the energy balance equation (Eq. (1)) at a time interval of interest requires knowledge of the values of climatic variables such as air temperatures, atmosphere relative humidities, and wind speeds at the same or similar time intervals. However, weather stations do not always provide standard data at time intervals of interest. Thus, diurnal changes in these variables need to be calculated from available daily average values using meteorological models (e.g., Ephrath et al., 1996). In this study, we compared relatively simple approaches for generating the diurnal cycles of climatic variables from available daily information.

Air temperature

Continuous values for air temperature, T_a, can be obtained from the daily maximum and minimum air temperatures usually available from the weather station using a trigonometric function with a period of 24 h as follows (Kirkham and Powers, 1972):

$$T_a = \bar{T} + A_t \cdot \cos\left[2\pi\left(\frac{t-13}{24}\right)\right] \quad (2)$$

where $\bar{T}$ is the average daily temperature (°C), A_t is the amplitude of the cosine wave (°C) calculated from the difference between the daily maximum and minimum temperatures, and t is a local time during the day (h). The argument of the cosine function shows that the highest temperature is assumed to occur at 1 p.m. and the lowest at 1 a.m.

Wind speed

It is well known that wind transports heat and effectively mixes the soil–atmospheric boundary layer. Wind is generally highly variable in speed and direction, since it involves mostly turbulent flow characterized by random fluctuations (Campbell, 1977). Because several parameterization formulas for components in the energy balance equation require continuous inputs of the wind speed, continuous diurnal changes of the wind speed must somehow be calculated even when daily average values are all that is available. At present we have two simple approaches, in addition to using a constant daily value for the entire day. Both approaches use the following maximum to minimum wind speed ratio U_r, which is defined as

$$U_r = \frac{U_{\max}}{U_{\min}} \quad (3)$$

where U_{max} and $U_{\min}$ (m s^{-1}) are the unknown minimum and maximum wind speeds of the day, respectively. This ratio may be determined from prior knowledge or calibration using available data. The maximum and minimum wind speeds can then be calculated from the daily average wind speed as follows:

$$U_{\max} = \frac{2U_r}{1+U_r}U \quad (4)$$

$$U_{\min} = \frac{2}{1+U_r}U \quad (5)$$

where U (m s^{-1}) is the daily average wind speed.

FAO (1990) simply used the maximum and minimum values for day-time (0700–1900) and night-time (1900–0700) wind speeds. On the other hand, Gregory (1989) modeled the cyclic behavior of the wind speed U_h during the day as follows:

$$U_h = U + (U_{\max} - U) \cdot \cos\left[2\pi\left(\frac{t - t_{\max}}{24}\right)\right] \quad (6)$$

where t is the time of the day and $t_{\max}$ is the time when the maximum wind speed occurs. In Gregory's study, the maximum wind speed occurred at 3:30 pm.

Relative humidity

Since typical diurnal air temperature variations show a cyclic behavior throughout the day, it is reasonable to assume that the relative humidity also shows such a cyclic pattern. As for the air temperature (Eq. (2)), a trigonometric function can be used to calculate continuous values of the relative humidity from the daily information (e.g., Gregory et al., 1994). When both the daily maximum and minimum relative humidity values are available, diurnal cycles of relative humidity can be generated using a cosine function with a period of 24 h as follows:

$$H_r = \bar{H} + A_r \cdot \cos\left[2\pi\left(\frac{t - t_{\max}}{24}\right)\right] \quad (7)$$

where $\bar{H}$ is the average daily relative humidity (–), A_r is the amplitude of the cosine wave calculated from the difference between the maximum and minimum relative humidity values, t is the local time within the day, and $t_{\max}$ is the hour of the day when the relative humidity is at its maximum. The relative humidity is generally at its minimum during day-time when the air temperature and the wind speed are at their maxima. Gregory et al. (1994) showed that the relative humidity was highest between 5 and 6 a.m. in Lubbock, Texas. In this study, we assume that the relative humidity peaks at 5 a.m.

In many cases, only daily average relative humidity values are available. The maximum and minimum relative humidity values can then be specified similar to those for wind speed, i.e., using the ratio of maximum and minimum values (Eq. (3)). After this ratio is determined, the maximum and minimum relative humidity values can be calculated, as with wind speed, using Eqs. (4) and (5). However, the maximum relative humidity value needs to be constrained so as not to exceed 100%. All values exceeding 100% need to be reset to 100%. The continuous diurnal cyclic change in the relative humidity can then be obtained using Eq. (7), in which the amplitude of the cosine wave can be obtained from the difference between the calculated maximum and minimum relative humidity values.

Parameterization of components in surface energy balance equation

Surface precipitation, irrigation, evaporation, and heat fluxes are used as boundary conditions for simulating soil water contents and temperatures in bare field soils. Evaporation and heat fluxes can be calculated from the surface energy balance, Eq. (1). Net radiation, R_n, is defined as (e.g., Brutsaert, 1982)

$$R_n = R_{ns} + R_{nl} = (1 - a)S_t + (\varepsilon_s R_{ld\downarrow} - R_{lu\uparrow}) \quad (8)$$

where R_{ns} is the net shortwave radiation (W m^{-2}), R_{nl} is the net longwave radiation (W m^{-2}), a is the surface albedo (–), S_t is the incoming (global) shortwave solar radiation (W m^{-2}), ε_s is the soil surface emissivity (–) representing the reflection of longwave radiation at the soil surface, $R_{ld\downarrow}$ is the incoming (thermal) longwave radiation at the soil surface (downward flux) (W m^{-2}) as emitted by the atmosphere and cloud cover, and $R_{lu\uparrow}$ is the sum of the outgoing (thermal) longwave radiation emitted from the surface (vegetation and soil) into the atmosphere (W m^{-2}).

Shortwave radiation

The value of the incoming shortwave solar radiation S_t (W m^{-2}), at any given time and location, can be calculated by taking into account the position of the sun (e.g., van Bavel and Hillel, 1976) using the following equation (Campbell, 1985):

$$S_t = \max(G_{sc} T_t \sin e, 0) \quad (9)$$

where G_{sc} is the solar constant (1360 W m^{-2}) and T_t (–) is the atmospheric transmission coefficient, which is defined as the ratio of the measured daily global solar radiation S_{tm} (W m^{-2}) and the daily potential global (extraterrestrial) radiation R_a (W m^{-2}):

$$T_t = \frac{S_{tm}}{R_a} \quad (10)$$

The last term of Eq. (9), e (rad), is the solar elevation angle given by (Monteith and Unsworth, 1990):

$$\sin e = \sin\varphi \sin\delta + \cos\varphi \cos\delta \cos\frac{2\pi}{24}(t - t_0) \quad (11)$$

where δ is the solar declination (rad), φ is the latitude (rad), t is the local time within a day, and t_0 is the time of solar noon.

Albedo

There are several accepted models to determine the surface albedo, a. A constant value can be applied for given surface conditions (e.g., 0.23 for grass). A simple linear relation relating albedo with the surface water content may also be used, since albedo depends, especially for bare soils, on the soil surface wetness. The following formula was proposed by van Bavel and Hillel (1976) to estimate the albedo as a function of the water content:

$$\begin{aligned} a &= 0.25 && \theta_0 < 0.1 \\ a &= 0.35 - \theta_0 && 0.1 \leqslant \theta_0 < 0.25 \\ a &= 0.10 && \theta_0 \geqslant 0.25 \end{aligned} \quad (12)$$

where θ_0 is the water content at the ground surface. In this function, the albedo is constant for low and high water contents, and varies linearly for intermediate water contents. On the other hand, in their study Kondo et al. (1992) used loam with a slightly different formula, where the albedo depends on the surface water content, even for dry conditions:

$$\begin{aligned} a &= 0.24 - 0.21\theta_0 && \theta_0 < 0.14 \\ a &= 0.35 - \theta_0 && 0.14 \leqslant \theta_0 < 0.22 \\ a &= 0.13 && \theta_0 \geqslant 0.22 \end{aligned} \quad (13)$$

Longwave radiation

Both incoming and outgoing thermal longwave radiations R_{ld} and R_{lu} in Eq. (8) need to be evaluated in order to obtain continuous net longwave radiation values. At a given temperature T (K), thermal longwave radiation is given by the Stefan–Boltzmann law (e.g., Jury and Horton, 2003):

$$\sum = \varepsilon\sigma T^4 \quad (14)$$

where σ is the Stefan–Boltzmann constant (5.67×10^{-8} W m^{-2} K^{-4} or 4.89×10^{-9} MJ m^{-2} K^{-4} d^{-1}), and ε is the emissivity (–), which is equal to 1 for a blackbody and has values between 0 and 1 for other surfaces. The net longwave radiation at any given time t can then be rewritten as (van Bavel and Hillel, 1976):

$$R_{nl}(t) = \varepsilon_s \varepsilon_a \sigma T_a^4 - \varepsilon_s \sigma T_s^4 \quad (15)$$

where subscripts a and s are used for the atmosphere and the soil, respectively.

The emissivity of the soil surface, ε_s, generally depends on the water content and vegetation of that surface. Although different empirical models are available for the emissivity of a soil surface with vegetation (i.e., surface emittance), soil surface emissivity usually has a value close to 1 (e.g., Ortega-Farias et al., 2000; Fuchs and Tanner, 1966). For bare soils without vegetation, the following two empirical models have been commonly used in the literature. The first formula (van Bavel and Hillel, 1976) gives the surface emittance of 0.9 for a dry surface and 0.98 for a saturated soil when the saturated water content is 0.45:

$$\varepsilon_s = 0.90 + 0.18\theta_s \tag{16}$$

Noborio et al. (1996b) used the following formula for the loamy sand, which gives nearly constant values for the surface emissivity for a range of water contents:

$$\varepsilon_s = 0.898 + 2.17 \times 10^{-2}\theta_s \tag{17}$$

Since water vapor and carbon dioxide in the air are the main emitting gases, the atmospheric emissivity ε_a depends on many other factors, such as the air temperature and the air humidity. In general, more than half of the longwave radiation received at the ground comes from gases in the lower 100 m of the atmosphere, and almost 90% comes from the first 1 km height (Monteith and Unsworth, 1990). Therefore, the longwave radiation can be calculated accurately if the profiles of the air temperature and the air humidity are known. However, that is rarely the case. To cope with this problem, a large number of parameterization methods have been developed empirically to estimate the atmospheric emissivity from the near-surface temperature and/or humidity, which are both commonly available and easily measured. While one set of formulas depends on both the surface air temperature and the surface air humidity, the other set is formulated as a function of the air temperature only. Some models of the former type are expressed as a function of the vapor pressure, e_a (kPa), or the vapor density, ρ_{va} (kg m^{-3}), both of which can be expressed conveniently as a function of the air temperature and the relative humidity of the air. The relative humidity is defined as either the ratio of the actual vapor pressure to the saturation vapor pressure, or the ratio of the actual vapor density to the saturation vapor density at a given temperature.

One of the first empirical models for calculating atmospheric emissivity was suggested by Brunt (1932). In this model, ε_a depends on the near-surface vapor pressure e_a (millibars) as follows:

$$\varepsilon_a = 0.51 + 0.066\sqrt{e_a} \tag{18}$$

Empirical coefficients in Brunt's formula were originally derived for a specific location. However, this relationship can be used for other locations, and can be thought of as a more-or-less universal equation (Hatfield et al., 1983). More recently, Chung and Horton (1987) used a similar formula that is a function of the vapor density, ρ_{va} (kg m^{-3}):

$$\varepsilon_a = 0.605 + 0.048\sqrt{1370 \cdot \rho_{va}} \tag{19}$$

One of the more-commonly used models is a power function originally derived by Brutsaert (1975):

$$\varepsilon_a = 1.24 \cdot \left(\frac{e_a}{T_a}\right)^{1/7} \tag{20}$$

where T_a is the near-surface air temperature (K). While Brutsaert's equation was derived from the physics of the process, the Brunt's equation is purely empirical. Because Brutsaert's model is fairly insensitive to changes in the air temperature, it can be simplified as follows (Brutsaert, 1975):

$$\varepsilon_a = 0.553 \cdot (e_a)^{1/7} \tag{21}$$

which corresponds to a typical air temperature of 285 K. Idso (1981) proposed a similar equation, in which the atmospheric emissivity depends on both T_a (K) and e_a (millibars), while also keeping the $e_a^{1/7}$ dependence:

$$\varepsilon_a = 0.179 e_a^{1/7} \exp(350/T_a) \tag{22}$$

Idso (1981) also proposed the following formula to avoid having a zero emissivity at the zero intercept in the above formula. The revised model has a linear dependency of ε_a on e_a:

$$\varepsilon_a = 0.70 + 5.95 \times 10^{-5} e_a \exp(1500/T_a) \tag{23}$$

Satterlund (1979) proposed the following equation to improve the estimation of atmospheric emissivity when the air temperature is below 0 °C:

$$\varepsilon_a = 1.08\left[1 - \exp\left\{-(e_a)^{T_a/2016}\right\}\right] \tag{24}$$

Other formulas that depend solely on the near-surface air temperature, T_a, were derived by Swinbank (1963) and Idso and Jackson (1969), respectively:

$$\varepsilon_a = 9.2 \times 10^{-6} T_a^2 \tag{25}$$

$$\varepsilon_a = 1 - 0.26 \exp\left\{-7.77 \times 10^{-4}(273 - T_a)^2\right\} \tag{26}$$

Evaporation and sensible heat flux

Since surface evaporation is controlled by atmospheric conditions, surface moisture, and water flow in the soil, a formula accounting for all of these factors is needed. Evaporation, E, in arid or semi-arid regions is often calculated as (Camillo and Gurney, 1986):

$$E = \frac{\rho_{vs} - \rho_{va}}{r_a + r_s} \tag{27}$$

where ρ_{vs} (kg m^{-3}) is the water vapor density at the soil surface, ρ_{va} (kg m^{-3}) is the atmospheric vapor density, r_a (s m^{-1}) is the aerodynamic resistance to water vapor flow from the soil surface to the atmosphere, and r_s (s m^{-1}) is the soil surface resistance to water vapor flow in soil pores acting as an additional (source of?) resistance coupled with the aerodynamic resistance (Camillo and Gurney, 1986).

Four variables need to be determined to calculate the evaporation rate using Eq. (27): ρ_{va}, ρ_{vs}, r_a, and r_s. The atmosphere vapor density ρ_{va} (kg m^{-3}) is obtained as:

$$\rho_{va} = \frac{RH}{100} \cdot \rho_{va}^* \tag{28}$$

where RH is the relative humidity of the air (%) and ρ_{va}^* is the saturated vapor density (kg m^{-3}), which can be expressed conveniently as a function of the air temperature (see for example, Campbell, 1977). The water vapor density at the soil surface is calculated following the equilibrium model of Philip and de Vries (1957) as:

$$\rho_{vs} = \exp\left[\frac{hMg}{RT_s}\right] \cdot \rho_{vs}^* \tag{29}$$

where ρ_{va}^* is the saturated vapor density at the soil surface (kg m^{-3}), h is the pressure head (m), M is the molecular weight of water (M mol^{-1}), g is the gravitational acceleration (m s^{-2}), T_s is the soil surface temperature (K), and R is the universal gas constant (J mol^{-1} K^{-1}) (8.314 J mol^{-1} K^{-1}).

The aerodynamic resistance, r_a, at the soil–atmosphere boundary is expected to vary depending upon the wind speed and the level of turbulence, which are determined by the roughness of the soil surface, the distance from the surface, and the condition of the atmosphere above the surface. The aerodynamic boundary layer resistance is commonly calculated as (Campbell, 1985):

$$r_a = \frac{1}{uk^2}\left[\ln\left(\frac{z_{ref}-d+z_H}{z_H}\right)+\psi_H\right] \cdot \left[\ln\left(\frac{z_{ref}-d+z_m}{z_m}\right)+\psi_m\right] \quad (30)$$

where k is von Karman's constant (=0.41), z_{ref} is the reference height of measurements (for both temperature and wind speed) (m), u is the mean wind speed (m s^{-1}) at height z_{ref}, d is the zero plane displacement (m), z_H is the surface roughness for the heat flux (m), z_m is the surface roughness for the momentum flux (m), ψ_H is the atmospheric stability correction factor for the heat flux (–), and ψ_m is the atmospheric stability correction factor for the momentum flux (–). For bare soils, the zero plane displacement, d, is equal to zero, while typical surface roughness values of 0.001 m are used for both z_H and z_m (Oke, 1978). Eq. (30) can be rewritten as:

$$r_a = \frac{1}{uk^2}\left[\ln\left(\frac{z_{ref}-d}{z_H}\right)+\psi_H\right] \cdot \left[\ln\left(\frac{z_{ref}-d}{z_m}\right)+\psi_m\right], \quad z_{ref} \gg z_H, z_m \quad (31)$$

when z_{ref} is much greater than the surface roughness (Brutsaert, 1982). In the remainder of the study, calculations are made using Eq. (31), because z_{ref} (1.5 m) is much greater than the typical roughness lengths for bare soils (e.g., 0.001 m).

The aerodynamic resistance depends on the so-called stability condition of the atmosphere, which can be assessed using Monin–Obukhov's stability parameter (or the MO length). The MO length is calculated as follows (e.g., Camillo and Gurney, 1986; Aluwihare and Watanabe, 2003):

$$\mathrm{MO} = -\frac{\rho_a c_a T_a U^{*3}}{kgH} \quad (32)$$

where H is the sensible heat flux at the soil surface, T_a is the atmosphere temperature (K) at z_{ref}, and U^* is the frictional velocity defined based upon the logarithmic wind profile law (e.g., Aluwihare and Watanabe, 2003; Camillo and Gurney, 1986; van de Griend and Owe, 1994; Brutsaert, 1982):

$$U^* = uk\left[\ln\left(\frac{z_{ref}-d}{z_m}\right)+\psi_m\right]^{-1} \quad (33)$$

The evaluations of ψ_m and ψ_h are then determined using the atmospheric stability parameter, ζ, defined as (Brutsaert, 1982):

$$\zeta = \frac{z_{ref}-d}{\mathrm{MO}} \quad (34)$$

For the neutral atmosphere, defined by the condition $|T_a - T_s| \leqslant 0.1$, the stability correction factors ψ_m and ψ_h become equal to 0 (e.g., Camillo and Gurney, 1986; Choudhury et al., 1986). For the unstable atmosphere ($T_a < T_s$ or MO < 0), the stability correction factors are empirically expressed as follows (e.g., Paulson, 1970; Brutsaert, 1982):

$$\psi_h = -2\ln\left(\frac{1+\sqrt{1-16\zeta}}{2}\right) \quad (35)$$

$$\psi_m = -2\ln\left(\frac{1+(1-16\zeta)^{0.25}}{2}\right) - \ln\left(\frac{1+\sqrt{1-16\zeta}}{2}\right) + 2\arctan\left\{(1-16\zeta)^{0.25}\right\} - \frac{\pi}{2} \quad (36)$$

and for the stable atmosphere ($T_a > T_s$ or MO > 0), the stability factors for the heat and momentum fluxes can be simply expressed as (for moderately stable, $\zeta < 1$, and extremely stable conditions, $\zeta > 1$):

$$\psi_h = \psi_m = \begin{cases} 5\cdot\zeta & 0<\zeta<1 \\ 5 & \zeta>1 \end{cases} \quad (37)$$

In general, calculations of r_a require an iterative procedure, as the stability factors are evaluated from variables that themselves depend on the stability factors. To avoid the iterative approach, Camillo and Gurney (1986) approximated the MO length as follows:

$$\mathrm{MO} = -\frac{\rho_a c_a T_a U^{*3}}{kgH} = \frac{T_a u^2}{g(T_a-T_s)\ln\left(\frac{z_{ref}}{z_0}\right)} \cdot \frac{1+\frac{\psi_h}{\ln(z_{ref}/z_0)}}{\left(1+\frac{\psi_m}{\ln(z_{ref}/z_0)}\right)^2} \approx \frac{T_a u^2}{g(T_a-T_s)\ln\left(\frac{z_{ref}}{z_0}\right)} \quad (38)$$

where z_h and z_m are assumed to be equal to the roughness length, z_0. They claimed that the right-hand-side portion of the third term of the above equation is always between 0.97 and 1.0 for their data, and may thus be set equal to 1.0. This results in there being no need for the iterative procedure.

A number of studies use the Richardson number, R_i, which is an alternative stability parameter (e.g., van Bavel and Hillel, 1976), in calculations of the aerodynamic resistance. The Richardson number can be estimated from (e.g., Brutsaert, 1982; Beljaars and Holtslag, 1991):

$$R_i = \frac{g\cdot(z_{ref}-d)\cdot(T_a-T_s)}{T_a\cdot u^2} \quad (39)$$

Like the aforementioned definition of the MO length, the atmosphere is stable when the Richardson number is positive, and unstable when the Richardson number is negative. The aerodynamic resistance is then defined using the neutral resistance, r_{aa} (when ψ_m and ψ_h are 0), and the stability correction ψ as:

$$r_a = r_{aa}\cdot\psi \quad (40)$$

Koivusalo et al. (2001) used the following stability correction parameter for stable and unstable conditions:

$$\psi = (1-10R_i)^{-1} \quad R_i < 0$$
$$\psi = (1+10R_i) \quad R_i > 0 \quad (41)$$

Unlike cases where the MO length is used, the Richardson number does not require an iterative approach, but allows direct estimation of the aerodynamic resistance. As can be seen from their definitions, the MO length (Eq. (32)) and the Richardson number (Eq. (39)) are strongly related, and there are a number of studies showing their relationship (e.g., Monteith and Unsworth, 1990).

On the other hand, the soil surface resistance, r_s, depends greatly on soil structure and texture. The relationship between r_s and the surface water content, θ_0, has been empirically formulated, typically using an exponential function (e.g., van de Griend and Owe, 1994), indicating that surface resistance increases dramatically as the soil dries out. A general formula for soil surface resistance was proposed by van de Griend and Owe (1994), for $\theta_0 \leqslant \theta_{\min}$:

$$r_s = r_0\exp(F(\theta_{\min}-\theta_0)) \quad (42)$$

where θ_0 is the soil water content (m^3 m^{-3}) in the top 1 cm, r_0 is the minimum surface resistance, which is theoretically equal to the resistance of the molecular diffusion across the water surface itself, $\theta_{\min}$ is the empirical minimum water content above which the soil is able to deliver vapor at a potential rate, and F is an empirical parameter. The following equation was fitted to the soil resistance data with the minimum resistance occurring at a soil water content of approximately 15% and an r_0 value of 10 (s m^{-1}):

$$r_s = \begin{cases} 10.0\cdot\exp(35.63(0.15-\theta_0)) & \theta_0 \leqslant 0.15 \\ 10.0 & \theta_0 > 0.15 \end{cases} \quad (43)$$

Camillo and Gurney (1986) used the formula for the surface resistance (s m^{-1}) originally proposed by Sun (1982):

$$r_s = 3.5\left(\frac{\theta_{sat}}{\theta_0}\right)^{2.3} + 33.5 \quad (44)$$

where θ_0 and θ_{sat} are the volumetric water contents in the top 0.5 cm of the soil, and at full saturation, respectively. One set of this data can also be represented very well by a linear model (correlation coefficient = −0.98):

$$r_s = -805 + 4140(\theta_{sat} - \theta_0) \quad (45)$$

Additional soil resistance formulas are cited by Mahfouf and Noilhan (1991). The Passerat de Silans' model has an exponential form as:

$$r_s = A\exp(B\theta_0) \quad (46)$$

where θ_0 is the soil water content ($m^3\ m^{-3}$) of the surface layer of specified depth (0–20 mm or 0–50 mm) and A and B are empirical parameters specific for the soil. In their study, the A and B parameters had values of 3.8113×10^{-4} and $-13.515/\theta_{fc}$, respectively, where θ_{fc} is the volumetric water content at field capacity. On the other hand, Kondo et al. (1990) proposed a different formula for sand, which is also a function of the water content:

$$r_s = \frac{F_1}{D_m}(\theta_{sat} - \theta_0)^{F_2} \quad (47)$$

where θ_0 is the soil water content ($m^3\ m^{-3}$) of the top 20-mm layer, F_1 and F_2 are fitting parameters with values of 8.32×10^5 and 16.6, respectively, and D_m is the molecular diffusion of water vapor, which has been formulated by Camillo et al. (1983) as:

$$D_m = D_0\left(\frac{T_s}{273.16}\right)^{1.75} = 0.229 \times 10^{-4}\left(\frac{T_s}{273.16}\right)^{1.75} \quad (48)$$

These parameter values were given by Kondo et al. (1990) for sand, which has a saturated water content of 0.392.

It is widely accepted that the aerodynamic resistance to vapor flow is usually very close to the aerodynamic resistance to heat flow (e.g., Aluwihare and Watanabe, 2003; van Bavel and Hillel, 1976). In this study, the sensible heat flux is thus calculated using the aerodynamic resistance (e.g., van Bavel and Hillel, 1976) as:

$$H = C_a\frac{T_s - T_a}{r_a} \quad (49)$$

where T_a is the air temperature (K), T_s is the soil surface temperature (K), and C_a is the volumetric heat capacity of air ($J\ m^{-3}\ K^{-1}$).

Numerical simulation

The modified HYDRUS-1D code used in this study solves the variably-saturated water flow and heat transport equations simultaneously (See Appendix), using the method of finite elements for the spatial discretization and finite differences for the temporal discretization (Saito et al., 2006). When the surface energy balance (Eq. (1)) is solved, the code can use either directly observed climatic data or the continuous diurnal values generated from available daily information. In this study, continuous diurnal values of climatic data were generated from daily information collected at the study site.

At each time step, the net radiation (R_n), the sensible heat flux (H), and the latent heat flux (LE) are calculated to obtain the surface heat flux (G) from the surface energy balance equation (Eq. (1)). The surface heat flux, G, is subsequently used as a known heat flux boundary condition. Calculations of R_n, H, and LE require knowledge of the temperature and pressure head at the soil surface. At a given time step, the energy balance equation is solved first with the heat flux at the boundary calculated using the soil moisture and temperature data obtained in a previous time step (old time step). Soil water contents are then updated using the resulting boundary water (evaporation) flux by solving Richards equation. The energy balance equation is then solved again, using updated soil water contents to obtain updated heat and water fluxes at the boundary. Finally, with updated boundary conditions, water flow and heat transport equations are solved. Convergence is checked after new soil moisture and temperature data are obtained.

Study site

The study site is a proposed low-level radioactive-waste disposal site in the Chihuahua Desert in West Texas, 10 km east of Sierra Blanca (31°8.773′ N, 105°16.237′ E; elevation 1337 m), where prototype engineering covers were installed (Scanlon et al., 2005). Engineered cover designs, with a conductive or capillary barrier of sand at the 2-m depth, were installed at the site in the summer of 1997. Water movement is generally restricted to only those zones above the capillary barrier in this type of cover. These covers also function as evapotranspiration (ET) covers, relying on surface vegetation to increase the water storage capacity of the covers by removing water through ET. As a result, drainage to deeper depths can be minimized and negligible. There was, however, no vegetation during the time period analyzed in this study.

The cover consists of 0.3 m of topsoil (sandy clay loam, bulk density of 1.5 $Mg\ m^{-3}$) underlain by 1.7 m of compacted soil (sandy clay loam, bulk density of 1.8 $Mg\ m^{-3}$). Gravel was added to the upper 0.3 m of the topsoil to reduce erosion. There is a 1.05 m capillary barrier underneath the compacted sandy clay loam layer, consisting of four layers: sandy loam, muddy gravel, gravel, and sand. The thicknesses of each layer are 0.3, 0.3, 0.3, and 0.15 m, respectively (Table 1).

Various hydrological and climatic data have been monitored at the site since October 1997. The monitoring system consists of an onsite weather station that monitors daily and hourly precipitation, wind speed, relative humidity, temperature, and solar and net radiations at 1.5 m above the surface. However, to test the performance of various meteorological models, continuous diurnal changes of climatic data were generated from daily information in this study.

Soil temperatures and pressure heads were measured at seven depths: 0.15, 0.3, 0.6, 0.9, 1.2, 1.5, and 2.0 m, using thermistors and heat dissipation sensors (Scanlon et al., 2002). Soil hydraulic properties of each soil layer were obtained from previous studies (Scanlon et al., 2002). Water retention data for soils in the upper three soil layers were based on laboratory measurements using a hanging water column (pressure heads from 0 to −2 m) and a

Table 1
Soil textures and soil hydraulic parameters for each layer of the ET cover at the study site (Scanlon et al., 2002).

Layer	Thickness (m)	Texture	K_s (cm/day)	θ_s	θ_r	α (cm^{-1})	n
1	0.3	Sandy clay loam	41	0.45	0.00	0.027	1.276
2	1.7	Sandy clay loam	20	0.35	0.00	0.010	1.167
3	0.3	Sand loam	639	0.40	0.00	0.020	1.464
4	0.3	Muddy gravel	10	0.14	0.00	0.007	1.188
5	0.3	Gravel	159840	0.51	0.00	10.95	1.722
6	0.15	Sand	587	0.38	0.00	0.050	1.774

Table 2
Parameters of Chung and Horton's (1987) soil thermal conductivity function for each layer of the ET cover at the study site.

Layer	b_1	b_2	b_3
1–3	0.244	0.393	1.534
4–6	0.228	−2.406	4.909

pressure plate apparatus (pressure heads from −1 to −50 m). Water retention data and saturated hydraulic conductivities for underlying soil layers were, on the other hand, obtained from various databases (e.g., UNSODA, Leij et al., 1996). Parameter values from Scanlon et al. (2002) for all six layers are summarized in Table 1. HYDRUS-1D default values for thermal conductivities were used for each layer of the soil profile based on its textural class: the thermal conductivity of loam for layers 1–3 and that of sand for layers 4–6 (Table 2).

Soil profile and initial conditions

The simulated soil profile is 3.05 m deep, with six soil layers. Seven observation nodes were defined in HYDRUS-1D, at depths where soil temperatures and pressure heads were measured. The soil profile was discretized using 103 nodes, with nodal spacing ranging from 0.2 cm near the soil surface and 2 cm around material interfaces to 15 cm within soil horizons. Simulations of the coupled transport of liquid water, water vapor, and heat were conducted to predict soil temperatures at each observation node for 365 consecutive days beginning October 1, 1997. There was no vegetation at the soil surface (i.e., bare soil) during this period (in August 1998, five perennial warm-season bunch grass species were planted). Initial conditions for temperatures and pressure heads are based on a linear interpolation of measured values at the site.

Boundary conditions

Boundary conditions at the soil surface for heat transport are determined from the surface energy balance equation. At any given time, the surface energy balance equation (Eq. (1)) is solved to obtain the surface heat flux, G, which is used as a known heat flux boundary condition. Precipitation and evaporation rates were used as upper boundary conditions for water flow. Zero pressure and temperature gradients were used as the bottom boundary conditions. These conditions assume that the water table is located far below the domain of interest, and that heat transfer across the lower boundary occurs only by convection of liquid water and water vapor.

Prediction performance

A set of meteorological models used in a previous study (Saito et al., 2006) was maintained as a combination of models used for reference. Models used for the reference run are listed in Tables 3–5 as Scenario 0. The impact of the choice of different meteorological models on predicted soil temperatures was then evaluated using the following procedure.

1. Select models to generate continuous diurnal values of the air temperature, the wind speed, and the relative humidity from daily climatic information.
2. Select models to calculate the soil albedo, the soil and atmospheric emissivities, and the aerodynamic and soil resistances.
3. For each selected model, specify parameter values.
4. Predict hourly soil temperatures numerically at seven observation nodes for the period of 365 days (from October 1, 1997 to September 30, 1998) using the modified HYDRUS-1D code with selected meteorological models with specified parameter values.

- Observation nodes are referred to as ON1 through ON7, from top (0.15 m depth) to bottom (2.0 m depth).

Table 3
Models used to generate continuous diurnal variations in air temperature, wind speed, and relative humidity. Bold font indicates the method's difference from the reference scenario.

Scenario	Air temperature	Wind speed	Ratio[a]	Relative humidity	Ratio[b]
0 (Reference)	Eq. (2)	Eq. (6)	3.0	Eq. (7)	3.0
1	Eq. (2)	**Eqs. (4) and (5)**	3.0	Eq. (7)	3.0
2	Eq. (2)	**Daily average**	–	Eq. (7)	3.0
3	Eq. (2)	Eq. (6)	3.0	Eq. (7)	**2.0**
4	Eq. (2)	Eq. (6)	3.0	**Daily average**	–

[a] Ratio of maximum and minimum wind speeds.
[b] Ratio of maximum and minimum relative humidity.

Table 4
Models used to calculate the albedo and the atmospheric and soil emissivities. For all scenarios listed in this table, the aerodynamic resistance model, r_a, given by Campbell (1985) is used. Bold font indicates the method's difference from the reference scenario. (vB&H – van Bavel and Hillel (1976), C&H – Chung and Horton (1987), I&J – Idso and Jackson (1969)).

Scenario	Albedo	ε_a	ε_s
0 (Reference)	Eq. (12) (vB&H)	Eq. (23) (Idso, 1981)	Eq. (16) (vB&H)
5	**Eq. (13) (Kondo et al., 1992)**	Idso	vB&H
6	**Constant (0.23)**	Idso	vB&H
7	vB&H	**Eq. (18) (Brunt, 1932)**	vB&H
8	vB&H	**Eq. (19) (C&H)**	vB&H
9	vB&H	**Eq. (20) (Brutsaert, 1975)**	vB&H
10	vB&H	**Eq. (21) (Brutsaert, 1975)**	vB&H
11	vB&H	**Eq. (22) (Idso, 1981)**	vB&H
12	vB&H	**Eq. (24) (Satterlund, 1979)**	vB&H
13	vB&H	**Eq. (25) (Swinbank, 1963)**	vB&H
14	vB&H	**Eq. (26) (I&J)**	vB&H
15	vB&H	Idso	**Eq. (17) (Noborio et al., 1996b)**

Table 5
Models used to calculate the aerodynamic and soil surface resistances. Bold font indicates the method's difference from the reference scenario. (C&G – Camillo and Gurney (1986), vG&O – van de Griend and Owe (1994), M&N – Mahfouf and Noilhan (1991)).

Scenario	r_a	r_s
0 (Reference)	MO, Eq. (38) (C&G)	Eq. (45) (C&G)
16	**MO, Eq. (32) (Iterative approach)**	C&G
17	**R_i, Eq. (41) (Koivusalo et al., 2001)**	C&G
18	C&G	**Eq. (44) (C&G)**
19	C&G	**Eq. (42) (vG&O)**
20	C&G	**Eq. (46) (M&N)**
21	C&G	**Eq. (47) (Kondo et al., 1992)**

- Day 1 corresponds to October 1, 1997 in the remainder of the manuscript.

5. At each observation node, x_j, compute the correlation coefficient between predicted and measured temperatures, and prediction errors: the mean square error (MSE) and the mean absolute error (MAE), which are defined, respectively, as follows:

$$\mathrm{MSE}_j = \frac{1}{N_j}\sum_{i=1}^{N_j}[T^*(x_j,t_i) - T(x_j,t_i)]^2 \quad (50)$$

$$\mathrm{MAE}_j = \frac{1}{N_j}\sum_{i=1}^{N_j}|T^*(x_j,t_i) - T(x_j,t_i)| \quad (51)$$

where N_j is the number of measurements at the x_j node, $T^*(x_j, t_i)$ represents the temperature measured at time t_i at the x_j node, and $T(x_j, t_i)$ is the corresponding predicted temperature.

- MSE is used to assess the overall prediction performance, while MAE is used to check discrepancies between observed and predicted temperature values.

6. Change one model at a time, and repeat from 1.

Since it is impractical to test all possible combinations of available meteorological models, we focus mainly on investigating what impact a change in a particular model has on soil temperature predictions, and not on finding the best combination of these models. We thus limit the number of combinations by starting with the reference combination (Table 3), and allowing only one model to change at a time. Table 3 shows models used to generate continuous diurnal changes in the wind speed and relative humidity. Models used in the calculation of the net radiation are listed in Table 4, while those used to obtain the surface resistances (soil and atmospheric) are summarized in Table 5. The remaining parameters, such as soil hydraulic and thermal properties, and initial and boundary conditions, are the same for the different scenarios.

Results and discussion

Generation of climatic data

Continuous diurnal changes in the air temperature can be generated using a sinusoidal function with a period of 24 h from daily maximum and minimum data (Kirkham and Powers, 1972). The formula (Eq. (2)) includes a term to allow the highest temperature to occur at 1 p.m. and the lowest at 1 a.m. Fig. 1 depicts the first 12 days of hourly measured air temperatures and those approximated from daily maximum and minimum values. Calculated air temperatures match observed values well, except for day 11. Because daily values were measured separately, they may not represent those of day 11 due to some problems in measurement.

Fig. 2 shows the first 12 days of diurnal wind speed hourly variations measured at the site, along with those calculated from the daily mean wind speed using different models. The simplest approach is to use the constant daily mean value. This approach obviously understates temporal variations of the wind speed, and may not be appropriate to simulate hourly variations of the soil temperature. When the FAO model (Eqs. (4) and (5)) is used, the day-time to night-time ratio needs to be specified. FAO recommends a ratio of about 2 for average conditions, which leads to a day-time wind speed 1.33 times greater than the mean value. Following the previous study of Saito et al. (2006), a ratio of 3 was used in this study. When $U_r = 3$, the day-time wind speed is 1.5 times greater than the mean value. Generated wind speeds approximate the observed values reasonably well, although detailed fluctuations were not modeled (Fig. 2). An obvious disadvantage of the FAO model is that there is always a sudden change in wind speed at 7 a.m. and 7 p.m., which may cause undesired consequences when the obtained value is used to calculate other climatic variables.

On the other hand, the Gregory's model allows for smoothly varying wind speed variations by applying a trigonometric function (Eq. (6)). The maximum to minimum wind speed ratio, equal to 3, was applied as in the FAO model above. Calculated wind speeds indeed change smoothly and approximate better observed wind speeds. Detailed fluctuations were again not modeled. Reproduction of such fluctuations can never be obtained using these simplified methods. Overall, both the FAO and Gregory's models approximate the general trend of the wind speed throughout the day from the mean daily value well.

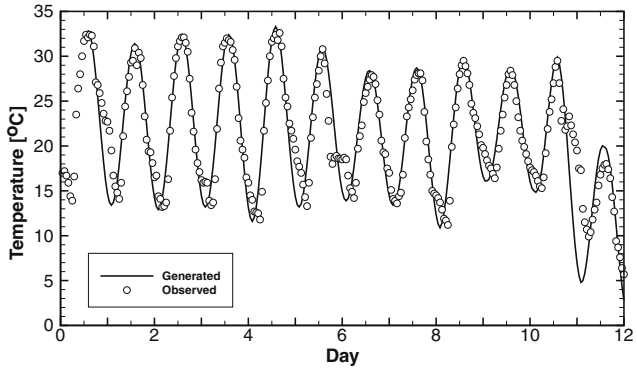

Fig. 1. Hourly variations of observed air temperatures at the study site (open circles) and those approximated from daily maximum and minimum values (solid line).

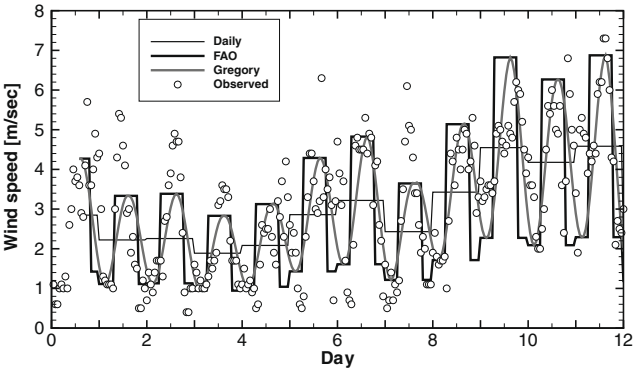

Fig. 2. Hourly variations of observed wind speeds at the study site (open circles) and those calculated from daily mean values using different models. In addition to daily mean values, the FAO model with day-time to night-time ratios of 2, and the Gregory model with the maximum to minimum ratio equal to 3 are compared. Time of the maximum wind speed is set to 3 pm.

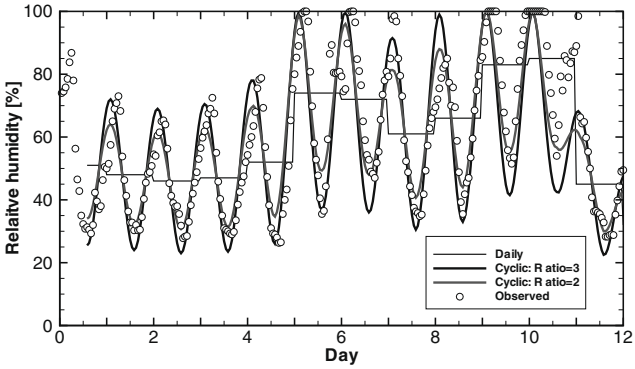

Fig. 3. Hourly variations of observed relative humidities at the study site (open circles) and those calculated from daily mean values. The maximum to minimum ratios of 2 and 3 are used with the peak time set to 5 a.m. Interpolated daily mean values are also displayed.

The generation of hourly variations of the atmospheric relative humidity from daily mean values requires a maximum to minimum relative humidity ratio that is similar to the one required for wind speed generation (Eq. (3)). Following the analysis of wind speed presented above, relative humidities calculated using ratios of 2 and 3 were compared with daily mean values and hourly measured values (Fig. 3). Relative humidities calculated using a ratio of 3 match the measured values well, especially around the measured maximums (i.e., 5 a.m.), while those calculated with the ratio of 2 fit the observed values well around the measured minimums (i.e., 5 p.m.). Daily mean values clearly underestimate temporal cyclic patterns of relative humidity. As can be observed in Fig. 3, relative humidity values can reach 100%, which leads to calculations of evaporation rates and heat fluxes that are numerically unstable. This is because having 100% relative humidity reverses the gradient in Eq. (27), even when the soil surface is relatively wet and predicted evaporation is equal to zero. However, in reality, the atmosphere is always mixing, and evaporation from the wet soil surface rarely stops completely. To avoid such conditions, the maximum atmospheric relative humidity in the program was set to 99.5% to allow soil water to evaporate even when the atmospheric humidity is near saturation.

Climatic variables

Net radiation calculations require values of the albedo, the soil emissivity, and the atmospheric emissivity at any given time. While albedo and soil emissivity can be computed using relatively simple equations, there is a great number of available and accepted formulas to calculate the atmospheric emissivity, as it is physically much more complicated than other climatic variables. Fig. 4 shows that different models provide quite different atmospheric emissivity values, especially for the low atmosphere humidity (i.e., 10%). As water molecules in the air are primary energy emittance sources, the atmospheric emissivity values increase with the relative humidity. When the relative humidity is 10%, the maximum difference among different formulas is about 0.4 (or 40%). Models that depend on both the air temperature and the relative humidity have, in general, similar trends; atmospheric emissivity values increase almost linearly as the air temperature increases. Slopes of these quasi-linear lines are quite similar. The two models that depend only on the air temperature provide much higher atmospheric emissivity values than the other formulas when the relative humidity is small (Idso and Jackson, Eq. (25) and Swinbank, Eq. (26)). As the relative humidity increases, the difference between different models decreases. The relative humidity in arid

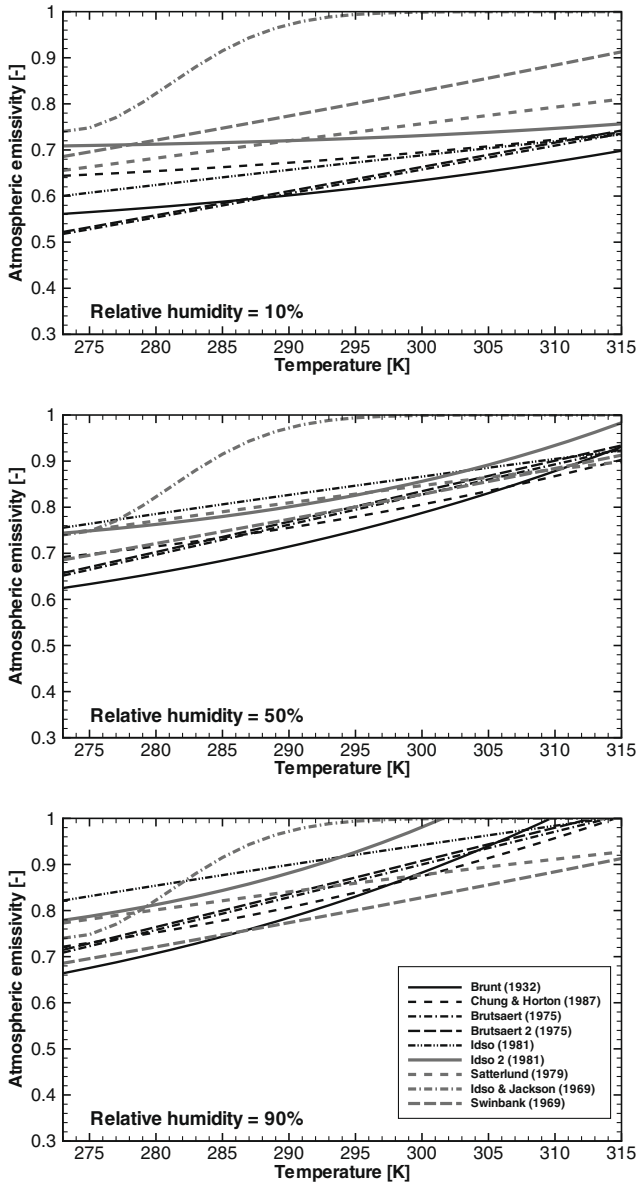

Fig. 4. The atmospheric emissivity obtained using 10 different models as a function of the air temperature (273–315 K) for three different relative humidity values: 10 (top), 50 (middle), and 90 (bottom)%.

or semi-arid regions can be very low and thus the choice of the atmospheric emissivity model may have an important impact on predictions of soil water contents and temperatures.

Soil temperature predictions

Different meteorological models mainly affect the various energy fluxes (e.g., reflection, emissivity, etc.) and their distribution during the day. Consequently, these models significantly affect predicted temperatures, while having only a limited affect on predicted pressure heads or water contents (especially at deeper depths), which showed only very small differences between different runs. Since simulated pressure heads and water fluxes at the study site were already extensively evaluated by Scanlon et al. (2002, 2005), in this section we will focus primarily on measured and predicted temperatures at different depths.

Predicted and observed soil temperatures at four observations nodes (ON1, 3, 5, and 7) are depicted in Fig. 5 for the Reference Scenario. Soil temperatures were predicted very well for the first 250

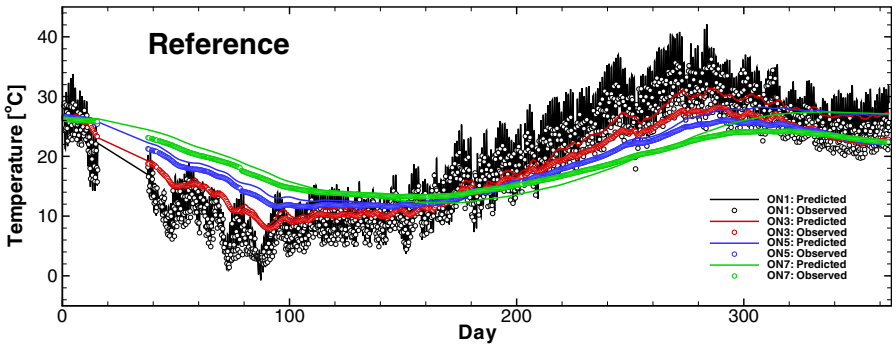

Fig. 5. Hourly temperature variations observed (open circles) at four observation nodes (ON1, 3, 5, and 7) during 365 days, along with those predicted using the Reference Scenario.

days, with the largest deviations within few temperature degrees. Despite some small discrepancies between the measured and predicted soil temperatures after 250 days, the overall agreement is reasonably good, considering that no calibration was involved, only default values of thermal properties were used, and only daily climatic information was used at input. Simulated soil temperatures

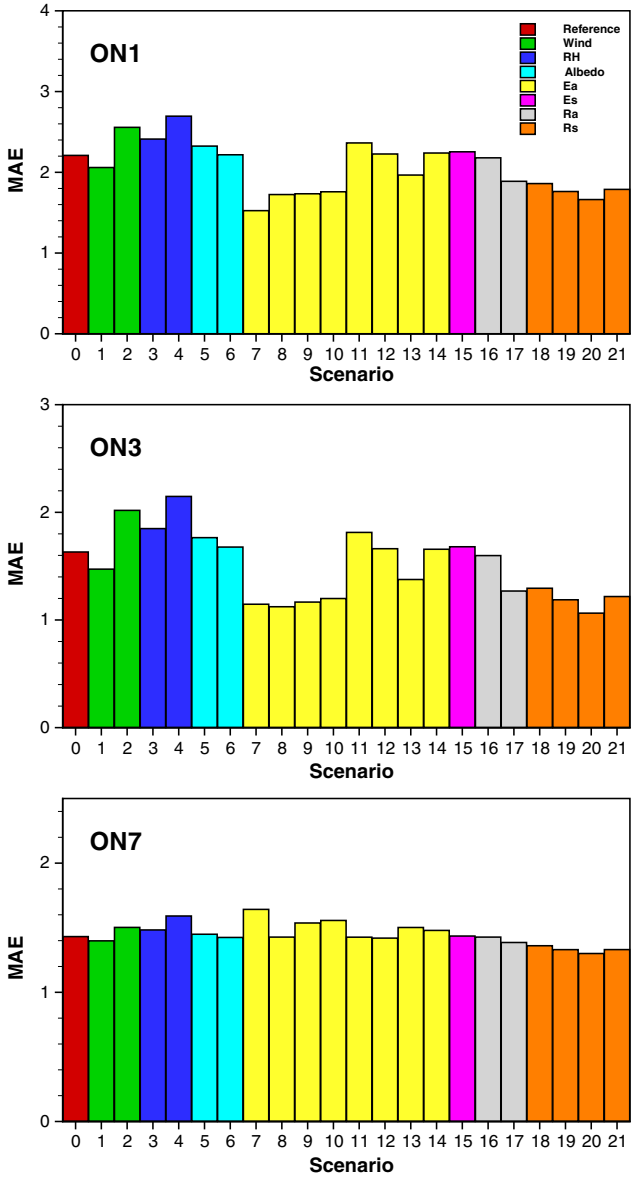

Fig. 6. Mean absolute errors (MAE) for soil temperatures at observation nodes 1, 3, and 7 for different scenarios.

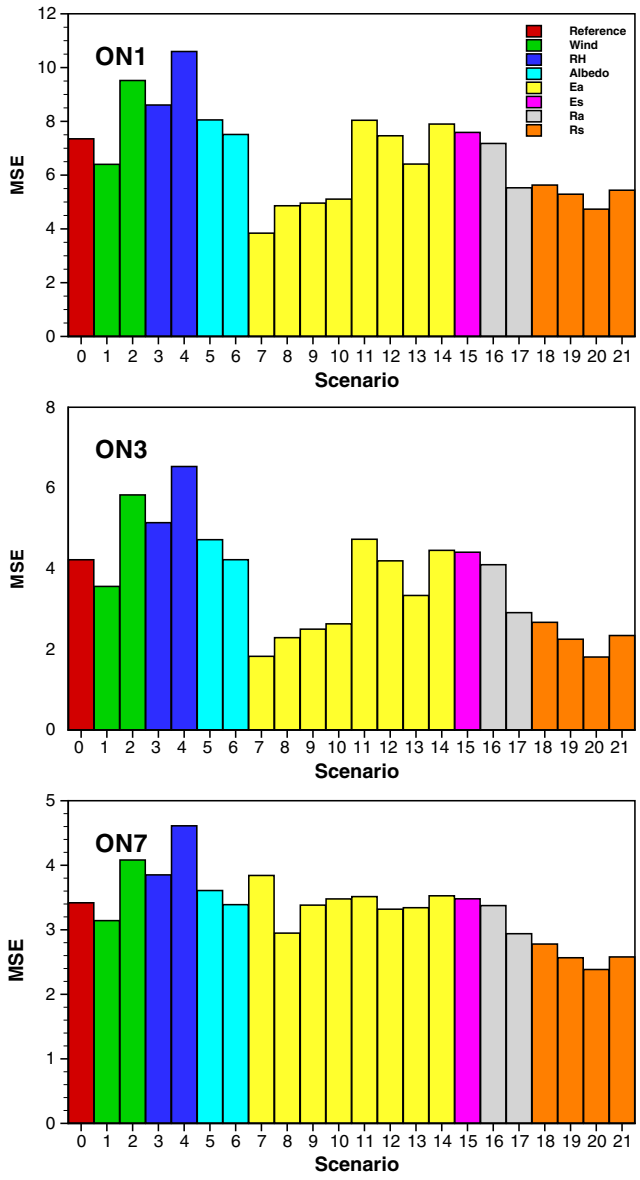

Fig. 7. Mean square errors (MSE) for soil temperatures at observation nodes 1, 3, and 7 for different scenarios.

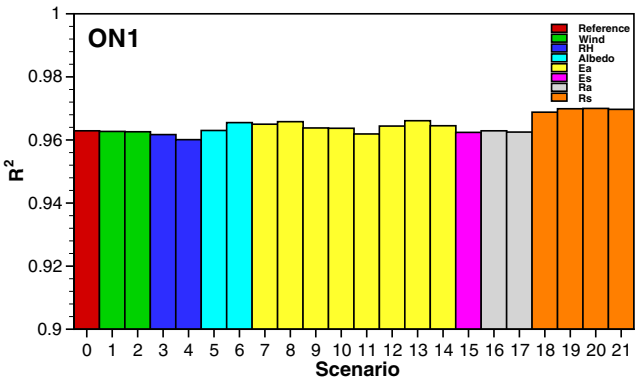

Fig. 8. Correlation coefficients (R^2) between observed and predicted temperatures at the observation node 1 (ON1) for different scenarios.

overestimate the observed values after 300 days, although discrepancies between observed and predicted temperatures are held within 5 °C, even at the 2-m depth, most of the time. The MAE at ON7 after 300 days increased to 3.54 °C, from the overall MAE of 1.43 °C. The reason for this overestimation after 300 days is unknown, but it may be associated with soil thermal properties that were not measured, but selected from the database based on the textural class. Diurnal fluctuations, as well as seasonal variations, are reproduced well at each observation node. Seasonal variations, or in other words annual fluctuations, are more important in deeper layers where there are almost no observed diurnal temperature changes. These variations are also more critical for the long-term simulations, which are important for the engineering cover performance assessment.

Mean absolute errors (MAE) and mean square errors (MSE) at observation nodes 1, 3, and 7 (i.e., at depths of 15, 60, and 200 cm, respectively) for all considered simulation scenarios are plotted in Figs. 6 and 7. Additionally, Fig. 8 shows the correlation coefficients between observed and predicted temperatures at all observation nodes for all simulation scenarios. For most scenarios, both MAE and MSE decrease from the upper node (ON1) to the lower node (ON7). Prediction errors decrease with depth, because temperature variations are damped in deeper layers, which lead to smaller variability in prediction errors. There are, however, several scenarios where MAE is greater at ON7 than at ON3. There is little difference in the MAEs at ON7, probably because the overestima-

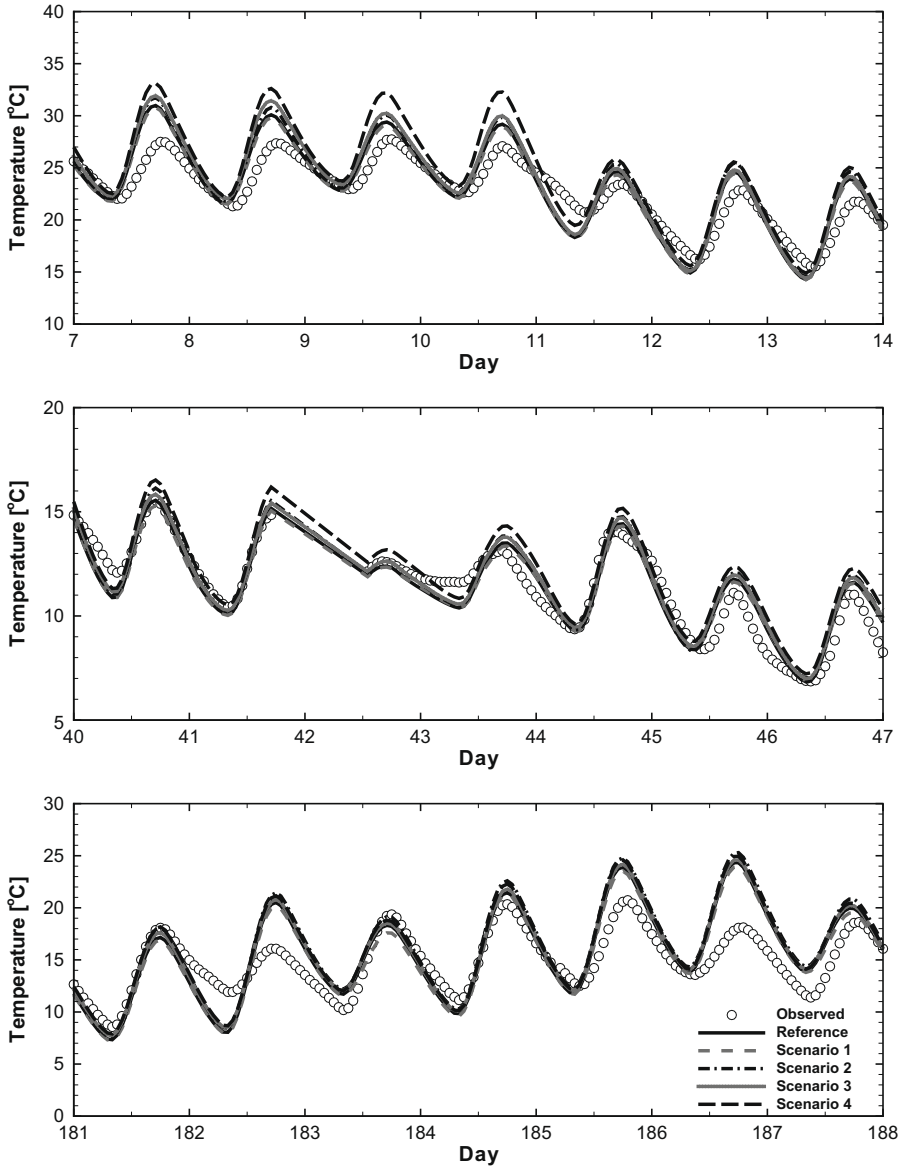

Fig. 9. Observed and predicted hourly temperature variations at ON1 for one week at three different periods (days 1–8, 51–58, 151–158). Different simulation scenarios (Reference, 1, 2, 3, and 4) are compared.

tion of the soil temperature after 300 days screens out small errors before day 300. This may also explain increases in MAEs for some scenarios at ON7 when compared to ON5. Some unexpected behavior at ON7 may also be due to the boundary effect, since ON7 is located on the boundary between layers 2 and 3, where the soil type changes from loam to gravel. Overall, however, the ranking of different scenarios based on errors is almost the same at different depths, except for the MSE at ON7. In other words, the propagation of errors at greater depths is independent of the choice of meteorological models. As the choice of models affects only the calculation of boundary conditions, errors induced at the surface boundary for a particular scenario simply propagate to deeper layers without being magnified or increased by errors from other sources.

Prediction errors calculated using the daily average values of the wind speed and relative humidity (Scenarios 2 & 4) are greater than those obtained with simple functions (Reference Scenario and Scenarios 1 & 3). Although improvements in predictions are relatively small in the long-term simulation, as depicted in Figs. 6 and 7, the results suggest that simple functions (e.g., Eq. (6)) used to generate these two climatic variables should be utilized when only daily average values are available. Although improvements in predictions seem to be much larger for short-term simulations that focus primarily on short-term variations of temperatures, as long as continuous values of air temperatures are obtained from a simple function (Eq. (2)), the improvements are relatively small (Fig. 9).

The impact of the choice of the albedo formula on temperature predictions is relatively small, as reflected by both MAE and MSE at all considered depths (Scenarios 5 & 6 in Figs. 6 and 7). It is obvious from Eqs. (12) and (13) that calculated albedo values are almost the same for different models when the soil surface is dry ($\theta < 0.1$), and such conditions were prevalent during most of the simulation time at the study site. Most accepted albedo models can thus be used for the bare soils of arid or semi-arid regions. This conclusion may, however, may not apply for humid conditions or for soil profiles with vegetation.

When an appropriate atmospheric emissivity model is selected, the prediction error can easily be reduced by 50% or more (compare Scenarios 7–14 with the Reference Scenario in Figs. 6 and 7). Among the various climatic variables considered in this study, models computing the atmospheric emissivity produce the widest range of values (Fig. 4). The Brunt equation (Eq. (18)), used in Scenario 7, leads to the smallest prediction errors and produces the

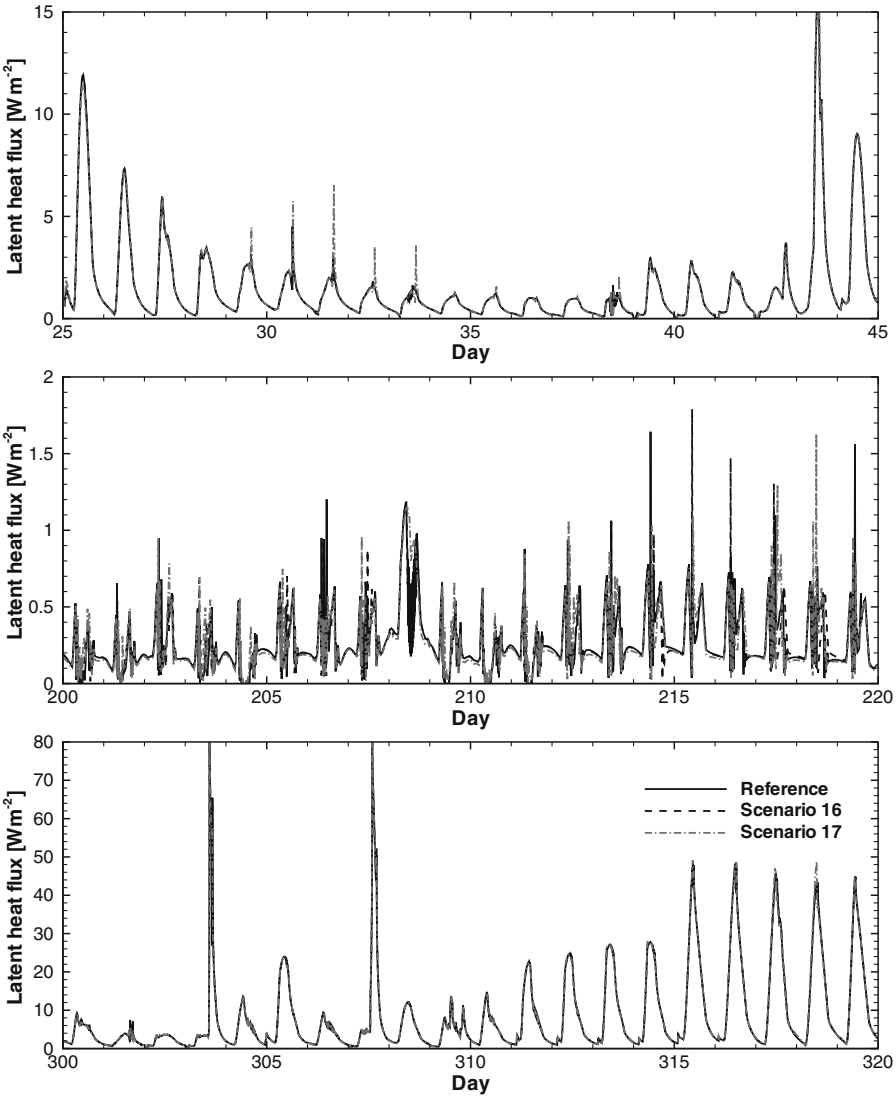

Fig. 10. Calculated hourly latent heat fluxes at the surface for 20-day time intervals at three different periods (days 25–45, 200–220, and 300–320). Different simulation scenarios (Reference, 16, and 17) are compared.

smallest atmospheric emissivity values for the large interval of relative humidity and temperature values, except when both relative humidity and temperature are high (Fig. 4). The higher the atmospheric emissivity, the more incoming longwave radiation from the atmosphere reaches the soil surface, and vice versa. There is no obvious explanation why the Brunt equation works better than the other formulas for this site. Although models that depend only on the temperature (Eqs. (25) and (26)) should not necessarily be excluded because of their relatively poor prediction performance in our study, those that depend either on the atmospheric pressure or the vapor density (Eqs. (18)–(24)) are likely to produce better predictions.

Two models that calculate the soil emissivity (Eqs. (16) and (17)) were compared. As expected, because of their similarity, there is no apparent difference in prediction errors between the Reference Scenario and Scenario 15 in Figs. 6 and 7.

Estimation of evaporation rates requires that more parameters be determined in comparison to other climatic variables. There is no distinct difference in prediction errors between the approximate approach (the Reference Scenario) and the iterative approach (Scenario 16) when the MO length is used in aerodynamic resistance calculations. This implies that there is no need to use the iterative approach, which demands more computational effort, for the long-term simulations. Both MAE and MSE for the scenario using the Richardson number (Scenario 17) are consistently smaller than those of the Reference Scenario, at all depths. Fig. 10 shows the calculated latent heat fluxes for three scenarios at the soil surface for three 20-days periods. Except for some minor fluctuations observed when latent heat fluxes are relatively small (from day 200 to day 220), the three scenarios are comparable regardless of the magnitude of latent heat fluxes. This demonstrates that the MO stability correction is no more accurate than the simpler method. Because of its simplicity, the approach that uses the Richardson number may be preferable to the one using the MO length. This conclusion should be valid not only for this particular dataset, but for other sites as well.

Among different models calculating the soil surface resistance, r_s (Scenarios 18–21), the equation cited by Mahfouf and Noilhan (1991) outperforms the others with regard to prediction errors (Figs. 6 and 7). The empirical parameters used by Mahfouf and Noilhan (1991) also worked reasonably well for our study site. Although different in details, all the formulas considered in this study are in the exponential form, which partly explains relatively small differences in prediction errors.

The correlation coefficients, r^2, between the observed and predicted temperatures, all very high (greater than 0.95), can be used to assess agreement in the overall trend of model predictions. Even with relatively large errors, r^2 can be close to one if the general trend is predicted well. High r^2s for all scenarios indicate that although differences in meteorological models do not significantly affect the overall trend of predicted temperatures, they may shift the predicted values away from observed temperatures. This is confirmed in Figs. 11–13. One can see that the predicted temperatures using different meteorological models are more-or-less parallel. As previously mentioned, the ranking of different methods with depth remains almost the same as errors introduced at the soil–atmosphere interface are propagated to deeper layers. It seems that no additional errors are introduced as the simulations

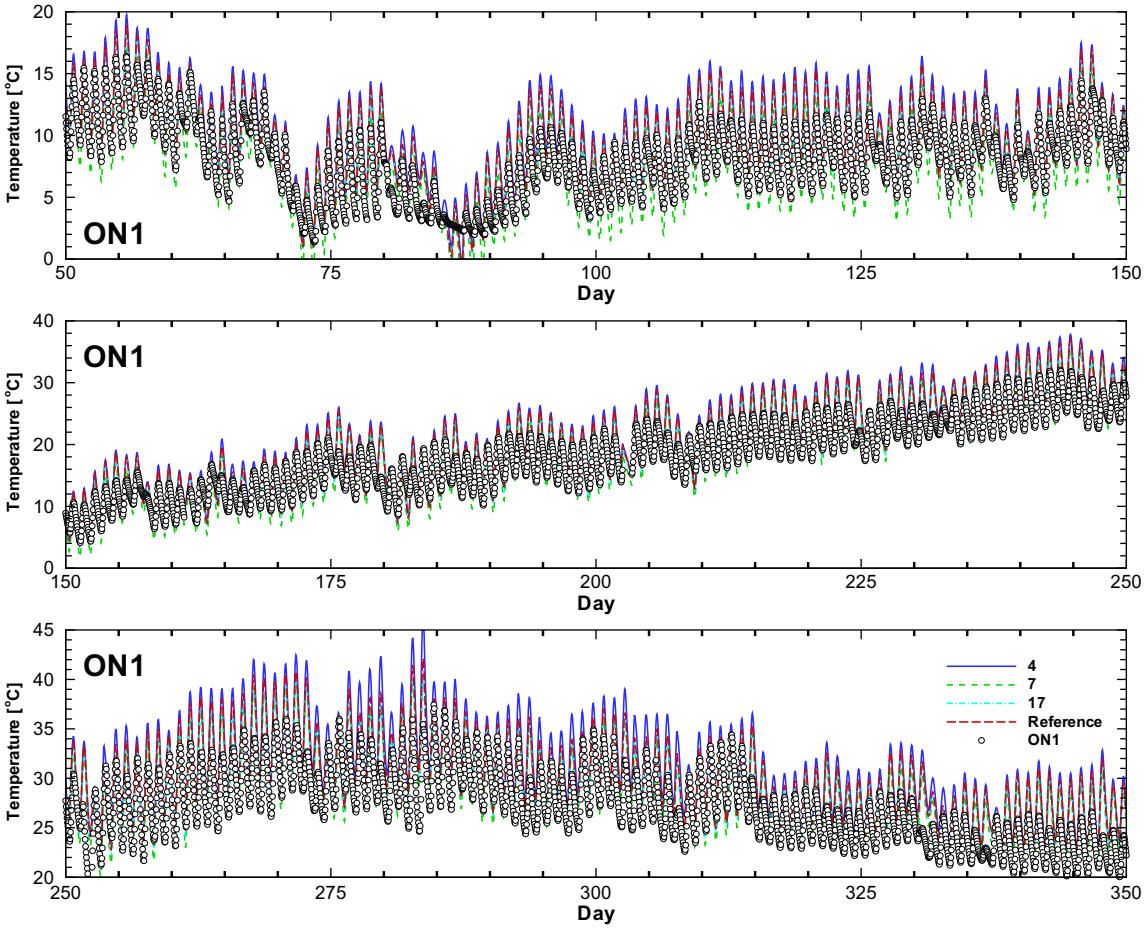

Fig. 11. Observed and predicted hourly temperature variations at ON1 from day 50 to day 365. Different simulation scenarios (Reference, 4, 7, and 17) are compared (notice different scales in different figures).

proceed. Although Figs. 11–13 show results for only three observation nodes, similar trends were observed at all depths.

Our results indicate that using more complicated models does not necessarily lead to better predictions of the soil temperature with depth than using simpler models. This conclusion should be applied to other sites as well. The majority of available meteorological models resulted in relatively good predictions of the soil temperature. However, we need to stress that the choice of meteorological models may lead to unwanted effects on temperature predictions, and thus needs to be done carefully. As important as it is to exert efforts to parameterize the soil hydraulic and thermal properties, determining the proper formulas for the components required to solve the energy balance equation is also essential.

Summary and conclusions

A complete evaluation of the soil thermal regime can be obtained by simulating the coupled movement of liquid water, water vapor, and heat energy in the subsurface. In our study, we modified the HYDRUS-1D software package to increase its flexibility in accommodating various types of climatic information, and to solve the coupled equations describing liquid water, water vapor, and heat transport in soils. Evaluation of the thermal regime of field soils requires, in addition to the solution of the subsurface water flow and heat transport equations, the solution of equations describing the surface water and energy balance. When only daily climatic information is available, available meteorological models need to be used to obtain continuous diurnal values of climatic data when solving the energy balance equation. The impact of the choice of such models on soil temperature predictions in the bare soil was investigated in this study. In addition, many different models for components used in the energy balance equation were compared. A variety of meteorological models were tested at the proposed low-level radioactive-waste disposal site in Chihuahua Desert in West Texas, where a thorough assessment of thermal conditions needs to be conducted. Different meteorological models were compared in terms of prediction errors of soil temperatures at seven observation depths.

Models used to generate diurnal cycles of the wind speed and the relative humidity were compared first. As expected, using daily average values led to greater prediction errors, while relatively simple extension methods could significantly improve soil temperature predictions. Models needed to obtain the net radiation were investigated next. While different models for the albedo and the soil emissivity had little impact on soil temperature predictions, the choice of the atmospheric emissivity model had a larger impact. Some methods could decrease prediction errors by 50% or more when compared to other methods. Soil and aerodynamic resistance models used in the calculation of the evaporation rate were tested last. As for the aerodynamic resistance, the model based on the Richardson number outperformed that using the Monin–Obukhov length. Comparable results were obtained for different soil resistance models, as all use similar exponential forms. A comparison of all the different meteorological models indicates that the error introduced at the soil–atmosphere inter-

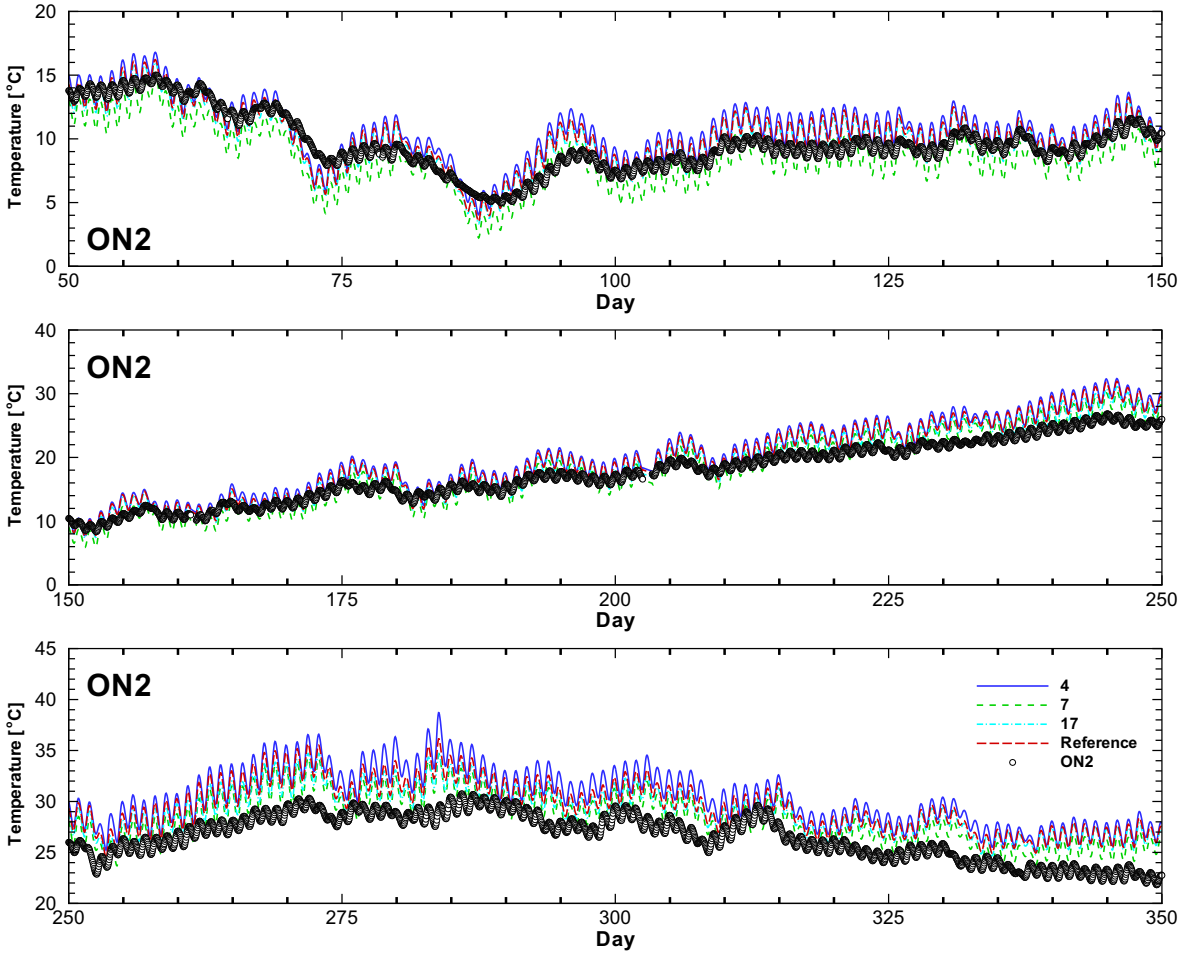

Fig. 12. Observed and predicted hourly temperature variations at ON2 from day 50 to day 365. Different simulation scenarios (Reference, 4, 7, and 17) are compared (notice different scales in different figures).

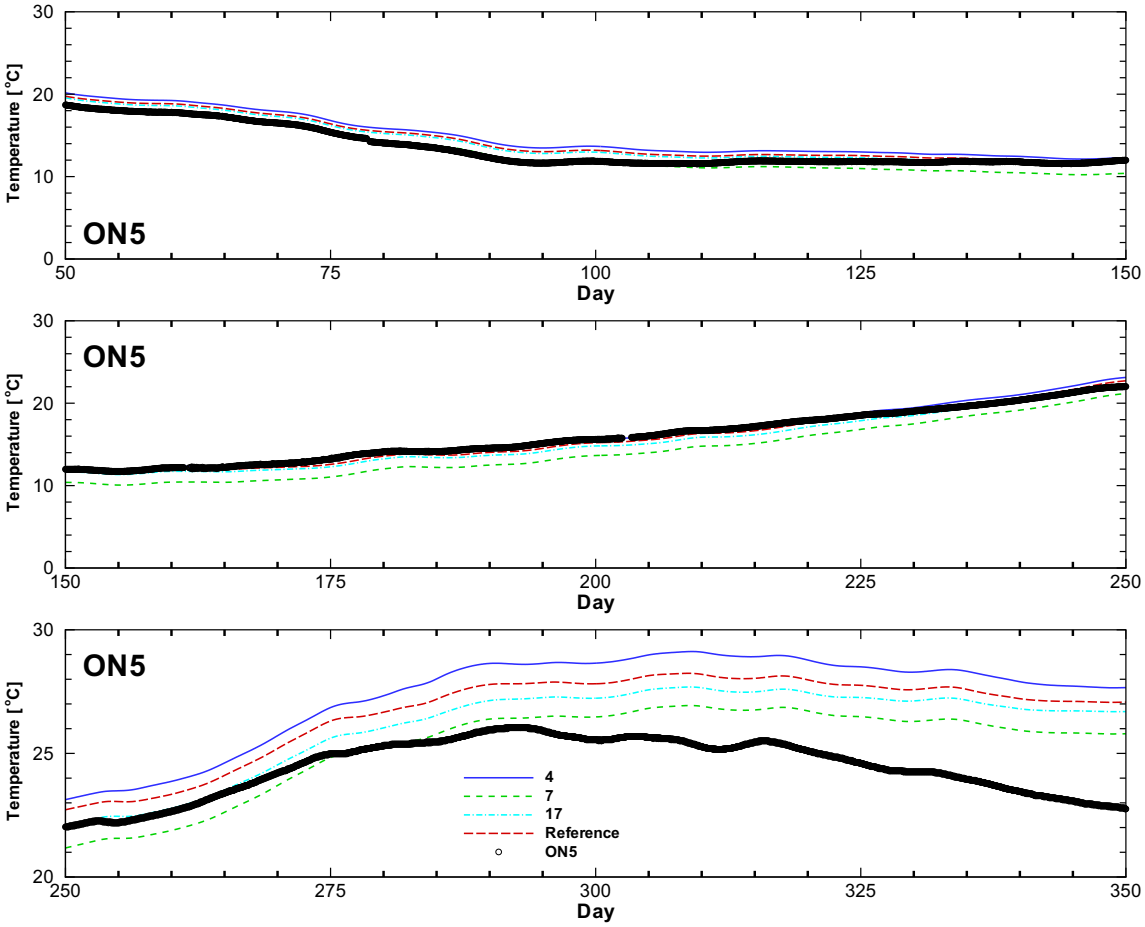

Fig. 13. Observed and predicted hourly temperature variations at ON5 from day 50 to day 365. Different simulation scenarios (Reference, 4, 7, and 17) are compared (notice different scales in different figures).

face propagates to deeper layers. In other words, the ranking of different methods does not change much for different depths.

We found that there is a best combination of meteorological models for this particular study site. However, the objective of our study was not to recommend the best combination of models to predict soil temperatures. It was rather to show quantitatively how the choice of meteorological models affects the soil temperature predictions. The results indicate that most of the meteorological models compared in this study can be used with confidence to solve the energy balance equation at the soil–atmosphere interface in coupled water, vapor, and heat transport models. Improvements in soil temperature predictions can be achieved not only by determining precisely the soil hydraulic and thermal properties, but also by selecting proper meteorological models to solve the surface energy balance equation. Most conclusions should hold not only for the site analyzed in this study, but for other sites where soil temperatures are to be predicted.

Acknowledgements

We would like to express our sincere gratitude to Bridget R. Scanlon for providing us with her soil temperature data. This paper is based on work supported in part by the BARD (Binational Agricultural Research and Development Fund) Project IS-3823-06 and by the National Science Foundation Biocomplexity programs #04-10055 and NSF DEB 04-21530. Financial support for the travel costs of the second author by the Japan Society for the Promotion of Science is greatly appreciated.

Appendix

The governing equations of variably-saturated water flow and heat transport in the vadose zone, as well as the soil hydraulic and thermal properties used in HYDRUS-1D are presented here. Details can also be found in Saito et al. (2006).

Coupled liquid water, water vapor, and heat transport

The governing equation for one-dimensional flow of liquid water and water vapor in a variably saturated rigid porous medium is given as follows:

$$\frac{\partial\theta}{\partial t}=\frac{\partial}{\partial z}\left[K_{Lh}\frac{\partial h}{\partial z}+K_{Lh}+K_{LT}\frac{\partial T}{\partial z}+K_{vh}\frac{\partial h}{\partial z}+K_{vT}\frac{\partial T}{\partial z}\right]-S$$
$$=\frac{\partial}{\partial z}\left[K_{Th}\frac{\partial h}{\partial z}+K_{Lh}+K_{TT}\frac{\partial T}{\partial z}\right]-S \quad (52)$$

where θ is the total volumetric water content ($m^3\ m^{-3}$), h is the pressure head (m), T is the temperature (K), z is the spatial coordinate positive upward (m), and S is a sink term usually accounting for the root water uptake (s^{-1}). K_{Lh} ($m\ s^{-1}$) and K_{LT} ($m^2\ K^{-1}\ s^{-1}$) are the (isothermal and thermal) hydraulic conductivities for liquid phase fluxes due to gradients in h and T, respectively, K_{vh} ($m\ s^{-1}$) and K_{vT} ($m^2\ K^{-1}\ s^{-1}$)

are the isothermal and thermal vapor hydraulic conductivities, respectively, and K_{Th} (m s^{-1}) and K_{TT} (m^2 K^{-1} s^{-1}) are the isothermal and thermal total hydraulic conductivities, respectively.

The governing equation for the movement of energy in a variably saturated rigid porous medium, on the other hand, is given as follows:

$$\frac{\partial C_p T}{\partial t} + L_0 \frac{\partial \theta_v}{\partial t} = \frac{\partial}{\partial z}\left[\lambda(\theta)\frac{\partial T}{\partial z}\right] - C_w \frac{\partial q_L T}{\partial z} - L_0 \frac{\partial q_v}{\partial z} - C_v \frac{\partial q_v T}{\partial z} - C_w S T \tag{53}$$

where C_w, C_v and C_p are volumetric heat capacities (J m^{-3} K^{-1}) of the liquid water, water vapor, and moist soil (de Vries, 1963), respectively, L_0 is the volumetric latent heat of vaporization of water (J m^{-3}), and the last term on the right side represents a sink of energy associated with root water uptake. $\lambda(\theta)$ is the apparent thermal conductivity of the soil (J m^{-1} s^{-1} K^{-11}), and q_L and q_v are the flux densities of liquid water and water vapor (m s^{-1}), respectively.

Model parameters

The pore size distribution model of Mualem (1976) was used to predict the isothermal unsaturated hydraulic conductivity function, K_{Lh}, from the saturated hydraulic conductivity K_s and the van Genuchten's (1980) model of the soil water retention curve:

$$\theta_l(h) = \begin{cases} \theta_r + \frac{\theta_s - \theta_r}{[1+|\alpha h|^n]^m} & h < 0 \\ \theta_s & h \geqslant 0 \end{cases} \tag{54}$$

$$K_{Lh} = K_S S_e^l [1 - (1 - S_e^{1/m})^m]^2 \tag{55}$$

where θ_s and θ_r are the saturated and residual water contents (m^3 m^{-3}), respectively, K_s is the saturated hydraulic conductivity (m s^{-1}), S_e is the effective saturation (–), and α (m^{-1}), n (–), m (=1 − 1/n), and l (–) are empirical shape parameters. The parameter l was given a value of 0.5 as suggested by Mualem (1976).

The thermal hydraulic conductivity function, K_{LT}, in Eq. (52) is defined as follows (e.g., Noborio et al., 1996b):

$$K_{LT} = K_{Lh}\left(hG_{wT}\frac{1}{\gamma_0}\frac{d\gamma}{dT}\right) \tag{56}$$

where G_{wT} is the gain factor, which quantifies temperature dependence of the soil water retention curve (Nimmo and Miller, 1986), γ is the surface tension of soil water (J m^{-2}), and γ_0 is the surface tension at 25 °C (=71.89 g s^{-2}).

The isothermal, K_{vh}, and thermal, K_{vT}, vapor hydraulic conductivities are described as (e.g., Nassar and Horton, 1989):

$$K_{vh} = \frac{D}{\rho_w}\rho_{vs}\frac{Mg}{RT}H_r \tag{57}$$

$$K_{vT} = \frac{D}{\rho_w}\eta H_r \frac{d\rho_{vs}}{dT} \tag{58}$$

where D is the vapor diffusivity in soil (m^2 s^{-1}), ρ_{vs} is the saturated vapor density (kg m^{-3}), M is the molecular weight of water (M mol^{-1}) (=0.018015 kg mol^{-1}), g is the gravitational acceleration (m s^{-2}) (=9.81 m s^{-2}), R is the universal gas constant (J mol^{-1} K^{-1}) (=8.314 J mol^{-1} K^{-1}), η is the enhancement factor (–) (Cass et al., 1984), and H_r is the relative humidity (–) (=RH/100).

The apparent thermal conductivity of the soil, $\lambda(\theta)$, in Eq. (53) combines the thermal conductivity of the porous media in the absence of flow, and the macrodispersivity which is assumed to be a linear function of the velocity (de Marsily, 1987). The apparent thermal conductivity, $\lambda(\theta)$, may then be expressed as (e.g., Šimůnek and Suarez, 1993):

$$\lambda(\theta) = \lambda_0(\theta) + \beta C_w |q|_l \tag{59}$$

where β is the thermal dispersivity (m). The thermal conductivity, $\lambda_0(\theta)$, accounts for the tortuosity of the porous medium, and can be described with a simple equation given by Chung and Horton (1987):

$$\lambda_0(\theta) = b_1 + b_2\theta + b_3\theta^{0.5} \tag{60}$$

where b_1, b_2, and b_3 are empirical regression parameters (W m^{-1} K^{-1}). Chung and Horton (1987) also provided average values for the b coefficients for three textural classes (i.e., clay, loam, and sand), which are implemented in the HYDRUS-1D program (Šimůnek et al., 1998).

References

Aluwihare, S., Watanabe, K., 2003. Measurement of evaporation on bare soil and estimating surface resistance. Journal of Environmental Engineering 129, 1157–1168.

Beljaars, A.C.M., Holtslag, A.A.M., 1991. Flux parameterization over land surfaces for atmospheric models. Journal of Applied Meteorology 30, 327–341.

Boulet, G., Braud, I., Vauclin, M., 1997. Study of the mechanisms of evaporation under arid conditions using a detailed model of the soil–atmosphere continuum. Application to the EFEDA I experiment. Journal of Hydrology 193, 114–141.

Brunt, D., 1932. Notes on radiation in the atmosphere. Quarterly Journal of the Royal Meteorological Society 58, 389–418.

Brutsaert, W., 1975. On a derivable formula for long-wave radiation from clear skies. Water Resources Research 11, 742–744.

Brutsaert, W., 1982. Evaporation into the Atmosphere: Theory, History, and Applications. D. Reidel Publishing Company, Dordrecht, The Netherlands.

Camillo, P.J., Gurney, R.J., 1986. A resistance parameter for bare-soil evaporation models. Soil Science 141, 95–105.

Camillo, P.J., Gurney, R.J., Schmugge, T.J., 1983. A soil and atmospheric boundary layer model for evapotranspiration and soil moisture studies. Water Resources Research 19, 371–380.

Campbell, G.S., 1977. An Introduction to Environmental Biophysics. Springer-Verlag, New York.

Campbell, G.S., 1985. Soil Physics with Basic, Transport models for soil–plant systems. Elsevier, New York.

Cass, A., Campbell, G.S., Jones, T.L., 1984. Enhancement of thermal water vapor diffusion in soil. Soil Science Society of America Journal 48, 25–32.

Choudhury, B.J., Reginato, R.J., Idso, S.B., 1986. An analysis of infrared temperature observations over wheat and calculation of latent heat flux. Agricultural and Forest Meteorology 37, 75–88.

Chung, S.-O., Horton, R., 1987. Soil heat and water flow with a partial surface mulch. Water Resources Research 23, 2175–2186.

de Marsily, G., 1987. Quantitative Hydrogeology, Groundwater Hydrology for Engineers. Academic Press, Inc., Orlando, FL.

de Vries, D.A., 1963. The thermal properties of soils. In: van Wijk, R.W. (Ed.), Physics of Plant Environment. North Holland, Amsterdam, pp. 210–235.

Ephrath, J.E., Goudriaan, J., Marani, A., 1996. Modelling diurnal patterns of air temperature, radiation, wind speed and relative humidity by equations from daily characteristics. Agricultural Systems 51 (4), 377–393.

FAO, 1990. FAO Penman-Monteith Formula. In Report: Expert consultation on revision of FAO methodologies for crop water requirement. May 28–31, Rome, Italy.

Fayer, M.J., 2000. UNSAT-H version 3.0: unsaturated soil water and heat flow model, theory, user manual, and examples. Rep. 13249. Pacific Northwest National Laboratory, Richland, Washington.

Fuchs, M., Tanner, C.B., 1966. Infrared thermometry of vegetation. Agronomy Journal 58, 597–601.

Gregory, J.M., 1989. Wind data generation for Great Plains locations. In: Proceedings of American Society of Agricultural Engineers, International Winter Meeting, December 12–15, New Orleans, LA.

Gregory, J.M., Peterson, R.E., Lee, J.A., Wilson, G.R., 1994. Modeling wind and relative humidity effects on air quality. In: International Conferences on Air Pollution from Agricultural Operations. Midwest Plan Service, Ames, IA, p. 183–190.

Hatfield, J.L., Reginato, R.J., Idso, S.B., 1983. Comparison of long-wave radiation calculation methods over the United States. Water Resources Research 19, 285–288.

Idso, S.B., 1981. A set of equations for full spectrum and 8- to 14-μm and 10.5- to 12.5-μm thermal radiation from cloudless skies. Water Resources Research 17, 295–304.

Idso, S.B., Jackson, R.D., 1969. Thermal radiation from the atmosphere. Journal of Geophysical Research 74, 5397–5403.

Jury, W.A., Horton, R., 2003. Soil Physics, sixth ed. John Wiley & Sons, Inc., New York.

Kirkham, D., Powers, W.L., 1972. Advanced Soil Physics. John Wiley & Sons, New York.

Koivusalo, H., Heikinheimo, M., Karvonen, T., 2001. Test of a simple two-layer parameterisation to simulate the energy balance and temperature of a snow pack. Theoretical and Applied Climatology 70, 65–79.

Kondo, J., Saigusa, N., Sato, T., 1990. A parameterization of evaporation from bare soil surface. Journal of Applied Meteorology 29, 385–389.

Kondo, J., Saigusa, N., Sato, T., 1992. A model and experimental study of evaporation from bare-soil surfaces. Journal of Applied Meteorology 31, 304–312.

Leij, F.J., Alves, W.J., van Genuchten, M.T., Williams, J.R., 1996. The UNSODA unsaturated soil hydraulic database, user's manual, version 1.0, EPA/600/R-96/095, Natl. Risk Manage. Lab., Off of Res. and Dev., Cincinnati, Ohio.

Mahfouf, J.F., Noilhan, J., 1991. Comparative study of various formulations of evaporation from bare soil using in situ data. Journal of Applied Meteorology 30, 1354–1365.

Monteith, J.L., Unsworth, M.H., 1990. Principles of Environmental Physics, second ed. Edward Arnold, London.

Mualem, Y., 1976. A new model for predicting the hydraulic conductivity of unsaturated porous media. Water Resources Research 12, 513–521.

Nassar, I.N., Horton, R., 1989. Water transport in unsaturated nonisothermal salty soil: II. Theoretical development. Soil Science Society of America Journal 53, 1330–1337.

Nimmo, J.R., Miller, E.E., 1986. The temperature dependence of isothermal moisture vs. potential characteristics of soils. Soil Science Society of America Journal 50, 1105–1113.

Noborio, K., McInnes, K.J., Heilman, J.L., 1996a. Two-dimensional model for water, heat, and solute transport in furrow-irrigated soil: I. Theory. Soil Science Society of America Journal 60, 1001–1009.

Noborio, K., McInnes, K.J., Heilman, J.L., 1996b. Two-dimensional model for water, heat, and solute transport in furrow-irrigated soil: II. Field evaluation. Soil Science Society of America Journal 60, 1010–1021.

Oke, T.R., 1978. Boundary Layer Climates. Methuen & Co Ltd., London.

Ortega-Farias, S., Antonioletti, R., Olioso, A., 2000. Net radiation model evaluation at an hourly time step for Mediterranean conditions. Agronomie 20, 157–164.

Paulson, C.A., 1970. The mathematical representation of wind speed and temperature profiles in the unstable atmospheric surface layer. Journal of Applied Meteorology 9, 857–861.

Philip, J.R., de Vries, D.A., 1957. Moisture movement in porous materials under temperature gradient. Transactions, American Geophysical Union 38, 222–232.

Saito, H., Šimůnek, J., Mohanty, B.P., 2006. Numerical analysis of coupled water, vapor, and heat transport in the vadose zone. Vadose Zone Journal 5, 784–800.

Satterlund, D.R., 1979. An improved equation for estimating long-wave radiation from the atmosphere. Water Resources Research 15, 1649–1650.

Scanlon, B.R., Christman, M., Reedy, R.C., Porro, I., Šimůnek, J., Flerchinger, G.N., 2002. Intercode comparisons for simulating water balance of surficial sediments in semiarid regions. Water Resources Research 38 (12), 1323. doi:10.1029/2001WR001233.

Scanlon, B.R., Reedy, R.C., Keese, K.E., Dwyer, S.F., 2005. Evaluation of evapotranspiration covers for waste containment in arid and semiarid regions in the southwestern USA. Vadose Zone Journal 4, 55–71.

Šimůnek, J., Suarez, D.L., 1993. The UNSATCHEM-2D code for simulating two dimensional variably saturated water flow, heat transport, carbon dioxide transport, and solute transport with major ion equilibrium and kinetic chemistry. Version 1.1. Research Report No. 128, US Salinity Laboratory, USDA, ARS, Riverside, California, 218pp.

Šimůnek, J., Šejna, M., van Genuchten, M.T., 1998. The HYDRUS-1D software package for simulating the one dimensional movement of water, heat, and multiple solutes in variably-saturated media. Version 2.0. IGWMC-TPS-70. International Groundwater Modeling Center, Colorado School of Mines, Golden, CO.

Sun, S.F., 1982. Moisture and heat transport in a soil layer forced by atmospheric conditions. MS Thesis, Dept. of Civil Engineering, University of Connecticut, 77 pp.

Swinbank, W.C., 1963. Long-wave radiation from clear skies. Quarterly Journal of the Royal Meteorological Society 89, 339–348.

van Bavel, C.H.M., Hillel, D.I., 1976. Calculating potential and actual evaporation from a bare soil surface by simulation of concurrent flow of water and heat. Agricultural Meteorology 17, 453–476.

van de Griend, A.A., Owe, M., 1994. Bare soil surface resistance to evaporation by vapor diffusion under semiarid conditions. Water Resources Research 30, 181–188.

van Genuchten, M.T., 1980. A closed-form equation for predicting the hydraulic conductivity of unsaturated soils. Soil Science Society of America Journal 44, 892–898.